



**Adjusting SiO<sub>2</sub>:C mole ratios in rice hull ash (RHA) to control carbothermal reduction to nanostructured SiC, Si<sub>3</sub>N<sub>4</sub> or Si<sub>2</sub>N<sub>2</sub>O composites.**

Journal:	<i>Green Chemistry</i>
Manuscript ID	GC-ART-06-2021-002084.R1
Article Type:	Paper
Date Submitted by the Author:	13-Aug-2021
Complete List of Authors:	Yu, Mengjie; University of Michigan, Temeche, Eleni; The University of Michigan, Materials Science and Engineering; University of Michigan, Material Science and Engineering Indris, Sylvio; Karlsruhe Institut fur Technologie, Institute for Applied Materials Laine, Richard; The University of Michigan, Macromolecular Science and Engineering Center

Adjusting SiO<sub>2</sub>:C mole ratios in rice hull ash  
(RHA) to control carbothermal reduction to  
nanostructured SiC, Si<sub>3</sub>N<sub>4</sub> or Si<sub>2</sub>N<sub>2</sub>O composites

*Mengjie Yu<sup>1</sup>, Eleni Temeche<sup>2</sup>, Sylvio Indris<sup>3</sup>, Richard M. Laine<sup>\*1,2</sup>*

<sup>1</sup>Macromolecular Science and Engineering, University of Michigan, Ann Arbor, MI  
48109, USA

<sup>2</sup>Department of Materials Science and Engineering, University of Michigan, Ann Arbor,  
MI 48109, USA

<sup>3</sup>Institute for Applied Materials-Energy Storage Systems (IAM-ESS), Karlsruhe Institute  
of Technology (KIT) Eggenstein-Leopoldshafen 76344, Germany

\*Corresponding Author

Richard M. Laine - [talsdad@umich.edu](mailto:talsdad@umich.edu)

Department of Materials Science and Engineering, and Macromolecular Science and Engineering,  
University of Michigan, University of Michigan, Ann Arbor, MI 48109-2136

## Abstract

We report here extracting SiO<sub>2</sub> as spiroxiloxane [(CH<sub>3</sub>)<sub>2</sub>C(O)CH<sub>2</sub>CH(O)CH<sub>3</sub>]<sub>2</sub>Si from rice hull ash (RHA) to carefully control the SiO<sub>2</sub>:C mole ratios, allowing direct carbothermal reduction to SiC, Si<sub>3</sub>N<sub>4</sub>, or Si<sub>2</sub>N<sub>2</sub>O without the need to add extra carbon and as a mechanism to preserve the original nanocomposite structure. We can adjust SiO<sub>2</sub>:C ratios from 2:15 to 13:35 simply by reacting RHA with hexylene glycol (HG) with catalytic base to distillatively extract SiO<sub>2</sub> to produce silica depleted RHA (SDRHA) with SiO<sub>2</sub> contents of 40-65 wt. % and corresponding carbon contents of 60-35 wt. % with specific surface areas (SSAs) up to 400 m<sup>2</sup>/g.

On heating SDRHA<sub>40-65</sub> at 1400-1500 °C in an Ar, N<sub>2</sub>, or N<sub>2</sub>-H<sub>2</sub> atmosphere, XRD patterns reveal formation of SiC, Si<sub>3</sub>N<sub>4</sub>, or Si<sub>2</sub>N<sub>2</sub>O as the major phase with some residual hard carbon. SEM studies reveal mixtures of particles and whiskers in the products, which show BET specific surface areas >40 m<sup>2</sup>/g after oxidative removal of excess carbon. Dilute acid and boiling water prewashing of RHA with milling eliminates typical product impurities compared to those found using conventional carbothermal reduction of agricultural wastes, which qualifies the resulting composites as components for electrochemical energy storage devices among other applications, to be reported elsewhere.

## Introduction

Commercially, most silicon carbide (SiC) and silicon nitride (Si<sub>3</sub>N<sub>4</sub>) production uses conventional carbothermal reduction or nitridation of SiO<sub>2</sub> by heating mixtures of quartz sand and carbon at >1900 °C.<sup>1-3</sup> Select efforts have explored replacing these starting materials with waste products, including natural sources such as rice husk and biomass,<sup>4-7</sup> and obsolete electrical appliances.<sup>8,9</sup> These sources can provide large quantities of SiO<sub>2</sub> or carbon, from which nanoscale reactants can be obtained by pre-treatment. As such, waste starting materials for fabricating SiC and Si<sub>3</sub>N<sub>4</sub> may offer several advantages: (1) the environmental benefits related to a reduced carbon footprint; (2) the economical disposal of waste materials; (3) improved properties arising from reduction of product particle sizes enabled by initiating production using nanoscale mixtures, and (4) economization of energy and capital equipment costs due to decreases in processing temperatures and times, etc.<sup>4,10-13</sup>

Rice is the second most-consumed food globally and is usually distributed in the market after polishing to remove rice hulls (RHs), which make up ~20 wt. % of as grown rice. RHs are generally considered agricultural waste since they have no obvious direct commercial uses. However, the discovery that they consist of 15-20 wt. % amorphous SiO<sub>2</sub> led to extensive efforts to produce SiC and Si<sub>3</sub>N<sub>4</sub> whiskers and particles.<sup>14-16</sup>

Lee and Cutler first used RHs to produce SiC in 1975.<sup>2</sup> Thereafter, a number of groups explored transforming RHs to SiC by heating at 1200-1500 °C under inert or reducing atmospheres.<sup>10,17,18</sup> In typical processes, RHs are first coked or ashed prior to conversion to SiC or Si<sub>3</sub>N<sub>4</sub>. Gorthy *et al.*<sup>19</sup> describe combusting RH at 280 °C in air to produce black ash with ~45 wt. % SiO<sub>2</sub>. Then, heating to 1500 °C/Ar converts this ash to SiC whiskers

(20 vol. %) 0.1-0.11  $\mu\text{m}$  diameters and 6-14  $\mu\text{m}$  particles (80 vol. %). Li *et al.*<sup>18</sup> heated RHs at 700 °C/Ar, then used microwave heating to generate 100-200 nm diameter whiskers and 60-130 nm particles. Similarly, Sujirote *et al.*<sup>20</sup> charred RHs at 1000 °C/Ar and then at 1500 °C/Ar producing SiC whisker and particle mixtures with 0.1-1  $\mu\text{m}$  diameters.

However, commercial manufacture of SiC and  $\text{Si}_3\text{N}_4$  from RHs has yet to be realized. Most RHs are disposed by burning, generating rice hull ash (RHA) used primarily to enrich soil to fertilize crops grown the next season.<sup>1,21,22</sup> The quantities of RH derived  $\text{SiO}_2$ , carbon, and residual mineral content vary depending on crop variety, growth climate, and location,<sup>23,24</sup> as well as the temperature and duration of combustion. Yeoh *et al.*<sup>25</sup> reported that amorphous  $\text{SiO}_2$  remained at combustion temperatures up to 900 °C for <1 h, while crystalline  $\text{SiO}_2$  formed at 1000 °C rapidly in 5 min. Hwang *et al.*<sup>26</sup> found greater  $\text{SiO}_2$  percentages in RHA and more volatile alkaline components at higher combustion temperatures.

Generally, RHA contains 80-90 wt. % amorphous  $\text{SiO}_2$ , while carbon and trace amounts of alkaline elements such as K, S, Ca, Mg comprise the remaining mass. Given the relatively high  $\text{SiO}_2$  content, only a limited number of studies report the synthesis of SiC and  $\text{Si}_3\text{N}_4$  from RHA.<sup>13,20,27,28</sup> Those reports, typically use RHA as the  $\text{SiO}_2$  source, adding an external carbon reactant. Thus, Li *et al.*<sup>27</sup> pyrolyzed a phenolic resin carbon source with RHA as a prelude to generating SiC nanowires. The RHA and resin mixture was embedded in graphite and then heated at 1600 °C. Chen *et al.*<sup>28</sup> used a graphene carbon source and template to grow SiC whiskers with diameters of 30-120 nm.

Likewise, excess carbon and coincidentally formed CO gas are essential in carbothermal nitridation producing  $\text{Si}_3\text{N}_4$ .<sup>29-31</sup> Abdulhameed *et al.*<sup>32</sup> combined RHA with sugarcane bagasse ash (carbon source), to synthesize  $\text{Si}_3\text{N}_4$  by reacting with  $\text{NH}_4\text{OH}$  via hydrothermal reaction. In other work, Pavarajarn *et al.*<sup>33</sup> detailed the carbothermal nitridation of RHA as a source of  $\text{Si}_3\text{N}_4$  fibers and whiskers. Although no extra carbon was added, the employed RHA contained only 45 wt. %  $\text{SiO}_2$ , which is suspected to be a feature originating from the growing environment (Thailand). It is evident that RHA with 80-90 wt. %  $\text{SiO}_2$  is not a viable starting point for these materials due to its quite low carbon content. However, this  $\text{SiO}_2$ :C ratio is rather typical of RHA sources worldwide, suggesting that carbon must be added to adjust stoichiometries that favor the formation of SiC and  $\text{Si}_3\text{N}_4$ . Thus, controlling the  $\text{SiO}_2$ :C ratios while retaining the intimately mixed carbon and  $\text{SiO}_2$  in the nanoscale is essential for more efficient use of RHA as a starting material for carbothermal reduction.

In addition to the variability of  $\text{SiO}_2$  and carbon contents in agricultural waste materials, another barrier hinders the commercial production of SiC and  $\text{Si}_3\text{N}_4$  from RH and/or RHA. As discussed above, most biomass and agricultural sources frequently contain significant quantities of impurities, closely affecting phases, morphologies, and purities of as-produced products.<sup>12,34</sup>

In light of the above background, the work presented here offers an alternate approach to the synthesis of SiC,  $\text{Si}_3\text{N}_4$ , and  $\text{Si}_2\text{N}_2\text{O}$  composites using acid purified RHA. Rather than introducing extra carbon, the ratio of  $\text{SiO}_2$ :C is optimized by distillative removal of  $\text{SiO}_2$  from RHA generating SDRHA with controllable  $\text{SiO}_2$ :C ratios. This process coincidentally and simply eliminates typical impurities providing starting

materials especially utile for carbothermal reduction reactions versus conventional agricultural sources.

## **Experimental Section**

### **Synthesis of SDRHA**

Rice hull ash (RHA) was a gift from Wadham Energy Inc. (Williams, CA). 2-Methyl-2,4-pentanediol (hexylene glycol) was purchased from ARCOS Organic, while potassium hydroxide (KOH) and hydrochloric acid (HCl) were purchased from Sigma-Aldrich (St Louis, MO), of which all were used as received.

The detailed analyses of RHA and impurity removal processes are reported elsewhere.<sup>35</sup> The as-received RHA was first milled in dilute hydrochloric acid (HCl) and repeatedly boiled in DI water to remove impurities. In a 2 L container, RHA (200 g) was milled with 200 g of yttria-stabilized zirconia sphere media (3 mm diameter) in HCl solution (0.1M). The RHA was milled for 48 h before being recovered by suction filtration through a Buchner funnel, which was then washed with 500 mL DI water. Then, the acid milled RHA was boiled for 24 h and separated by filtrating through a Buchner funnel. The boiling and filter processes were repeated until the pH of boiled water filtered off was neutral. Last, the RHA was dried at 100 °C/vacuum overnight prior to the silica-depleting reaction.

A mixture of 250 mL hexylene glycol (HG) and 4.2 g KOH (75 mmol) was first heated to 190 °C in a 250 mL three-neck flask equipped with a stir bar to remove water for 3 h. Dried RHA powders (~50 g) were added to the HG + KOH solution. The mixture was heated to 200 °C in a pyrex distillation setup. After 100 mL HG was distilled, another

100 mL HG was added. The dissolved  $\text{SiO}_2$  content was adjusted by controlling reaction times and HG volumes introduced to the reaction. For instance, after reacting with 100 mL HG in 24 h, SDRHA with  $\sim 70$  wt. %  $\text{SiO}_2$  was obtained. When heating is terminated and no more HG is added, the  $\text{SiO}_2$ :C ratios are fixed in the recovered SDRHA.

### **Production of SiC, $\text{Si}_3\text{N}_4$ , and $\text{Si}_2\text{N}_2\text{O}$ composites from SDRHA**

SDRHA powder was placed in a graphite crucible and covered with an alumina disk, which was then heated in a tube furnace (GSL-1700X, MTI Corporation). Heat-treatments were conducted at different temperatures and duration times at a heating rate of  $10^\circ\text{C}/\text{min}$ . Heating in atmosphere of Ar,  $\text{N}_2$ , and  $\text{N}_2$ - $\text{H}_2$  mixtures generates SiC,  $\text{Si}_3\text{N}_4$ , and  $\text{Si}_2\text{N}_2\text{O}$  composites, respectively, with some amounts of excess carbon, crystalline  $\text{SiO}_2$  and secondary Si-containing phases of the related compounds. Detailed discussions are found in the result section.

### **Characterization**

Fourier-transform infrared spectroscopy (FTIR) Nicolet 6700 Series FTIR spectrometer (Thermo Fisher Scientific, Inc.) was used to collect FTIR spectra. The samples were mixed with KBr (International Crystal Laboratories).  $\text{N}_2$  was purged in the chamber during data acquisition in the range of  $4000$ - $400\text{ cm}^{-1}$ .

X-ray diffraction (XRD) Rigaku Miniflex diffractometer (Rigaku Denki., LTD., Tokyo, Japan) with  $\text{Cu-K}\alpha$  radiation ( $k = 0.154\text{ nm}$ ) was used to identify the phases and characterize the crystallinity nature and phases of the RHA, SDRHA, SiC,  $\text{Si}_3\text{N}_4$ , and  $\text{Si}_2\text{N}_2\text{O}$  composites. The diffraction data were recorded in the  $2\theta$  over the ranges of  $10$ - $80^\circ 2\theta$  using a scan rate of  $5\text{ min}^{-1}$ . The presence of crystallographic phases and their wt. % fraction were refined using PDXL software (Version 2.8.4).

BET specific surface area (SSA) analyses Micromeritics ASAP 2020 sorption analyzer was used to measure the SSAs. Samples were degassed at 300 °C/6 h prior to analyses by N<sub>2</sub> physisorption at -196 °C (77 K). BET method using 10 data multipoint with relative pressures of 0.05-1 was applied. The pore volume was calculated based on the Barret–Joyner–Halenda (BJH) model.

Scanning electron microscopy (SEM) JSM-IT300HR In Touch Scope SEM (JEOL USA, Inc.) was used to acquire the microstructure images and EDX maps of RHA, SDRHA, SiC, Si<sub>3</sub>N<sub>4</sub>, and Si<sub>2</sub>N<sub>2</sub>O composites.

Thermogravimetric Analysis (TGA) Q600 simultaneous TGA/DSC (TA Instruments, Inc.) was used to determine the carbon content in RHA, SDRHA, SiC, Si<sub>3</sub>N<sub>4</sub>, and Si<sub>2</sub>N<sub>2</sub>O composites. Samples (10-20 mg) were placed in alumina pans and ramped to 600 °C at 10 °C min<sup>-1</sup> in the presence of air (60 mL min<sup>-1</sup>). The SiO<sub>2</sub>:C mole ratios of SDRHA are calculated from the molar mass and weight of each component as determined by TGA.

Magic-angle spinning (MAS) nuclear magnetic resonance (NMR) spectroscopy Bruker Avance 500 MHz spectrometer was used to conduct the solid-state NMR at a magnetic field of 11.7 T ( $\omega = 130.3$  MHz). Spinning (30 kHz) was performed in 2.5 mm zirconia rotors. A rotor-synchronized Hahn-echo pulse sequence was applied to acquire the spectra at a  $\pi/2$  pulse length of 2.7  $\mu$ s.

X-ray photoelectron spectroscopy (XPS) Kratos Axis Ultra (Kratos Analytical) was used to analyze the elements present. XPS system at room temperature under  $3.1 \times 10^{-8}$  Pa using monochromatic Al source (14 kV and 8 mA) was used to record the core level atoms. Binding energies of all the elements were calibrated relative to C 1s at 284.8 eV. Data was analyzed using CasaXPS software (Version 2.3.22PR1.0).

## Results and Discussion

Combustion followed by stoichiometric alkali treatment is the most common method of extracting  $\text{SiO}_2$  from RHA (1), generating extractable silicates as the product:<sup>23,36,37</sup>

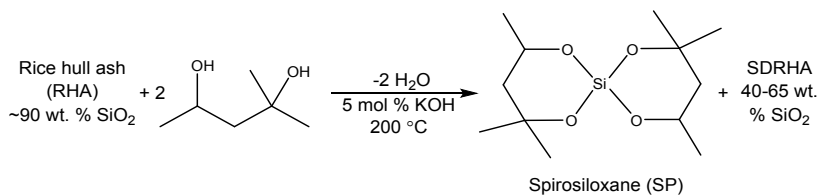


### Scheme 1. Conventional method of extracting $\text{SiO}_2$ from RHA.

However, this two-step process defeats the original advantage of intimate mixing of nanoscale carbon and  $\text{SiO}_2$  that enables low-cost production of  $\text{SiC}$  and  $\text{Si}_3\text{N}_4$  from RHA. Furthermore, any trace minerals present in the RHA remain in the SDRHA.

In principle, a more environmentally- and economically-friendly approach should eliminate these trace impurities, adjust the  $\text{SiO}_2$  content and limit the alkali metal amounts to reduce their presence as impurities. It is now well understood that milling RHA in dilute acid followed by washing with boiling water provides SDRHA with very low impurity levels to the point where it is now possible to process solar-grade silicon (99.999% pure) from this SDRHA;<sup>35</sup> however, in this previously developed process, carbon had to be added.

Most recently, we have resolved multiple problems of the types noted above by learning to remove  $\text{SiO}_2$  from RHA by forming spiroxiloxane (SP) per:<sup>38</sup>



### Scheme 2. Dissolution of $\text{SiO}_2$ from RHA allows distillative removal via spiroxiloxane.

We detailed the isolation and purification of distilled SP recently.<sup>38,39</sup> As water is used to dissolve the distilled HG and to separate it from SP, recycling the HG by removing water further highlights the prominent sustainability of this method, not to mention the low toxicity of HG. In addition, the base used as catalyst likely remains as  $K_2SiO_3$  and can also be recycled.

As just noted, SDRHA is a practical precursor to solar grade silicon (99.999 % pure).<sup>35</sup> Coincidentally, SP offers access to high surface area fumed  $SiO_2$  and precipitated  $SiO_2$  for vacuum insulation panels.<sup>40</sup> Recently, its utility was extended to high-performance electrodes for hybrid  $Li^+$  supercapacitors<sup>41</sup> and precursors for solid electrolytes.<sup>39</sup>

### Synthesis of SDRHA

The as-received RHA used contains ~90 wt. %  $SiO_2$ . Detailed SDRHA synthesis procedures are reported elsewhere and discussed in the experimental section.<sup>42</sup> Briefly, the first step is to mill the as-received RHA in dilute acid followed by washing with boiling water, which removes the majority of the mineral impurities.<sup>43,44</sup> The dried RHA is reacted with hexylene glycol using catalytic amounts of potassium hydroxide (Scheme 2), followed by washing to separate SDRHA. Figure 1a provides representative TGAs of acid-washed/dried RHA and SDRHA at 25-600 °C under air after distilling part, providing respective  $SiO_2$  contents. No apparent mass decrease is observed after oxidation of carbon finishes at ~480 °C, suggesting 60 wt. %  $SiO_2$  remains in the SDRHA<sub>60</sub>. Signature peaks for C 1s, Si 2s, Si 2p, and O 1s are shown in the XPS wide

survey spectra of SDRHA<sub>60</sub> in Figure 1b, indicating the removal of impurities from the raw materials.

The XRD patterns shown in Figure 1c indicate that RHA consists of amorphous SiO<sub>2</sub> and carbon before and after SiO<sub>2</sub> extraction, while EDX analyses (Figure 1d) confirm intimate mixing of SiO<sub>2</sub> and carbon in SDRHA (60 wt. % SiO<sub>2</sub>, denoted SDRHA<sub>60</sub>) at nanoscales. As such, the essential conditions for effective carbothermal reduction at relatively low temperatures, *i.e.* milling of amorphous SiO<sub>2</sub> and carbon sources in traditional manufacturing processes,<sup>23,45,46</sup> are met without extra effort.

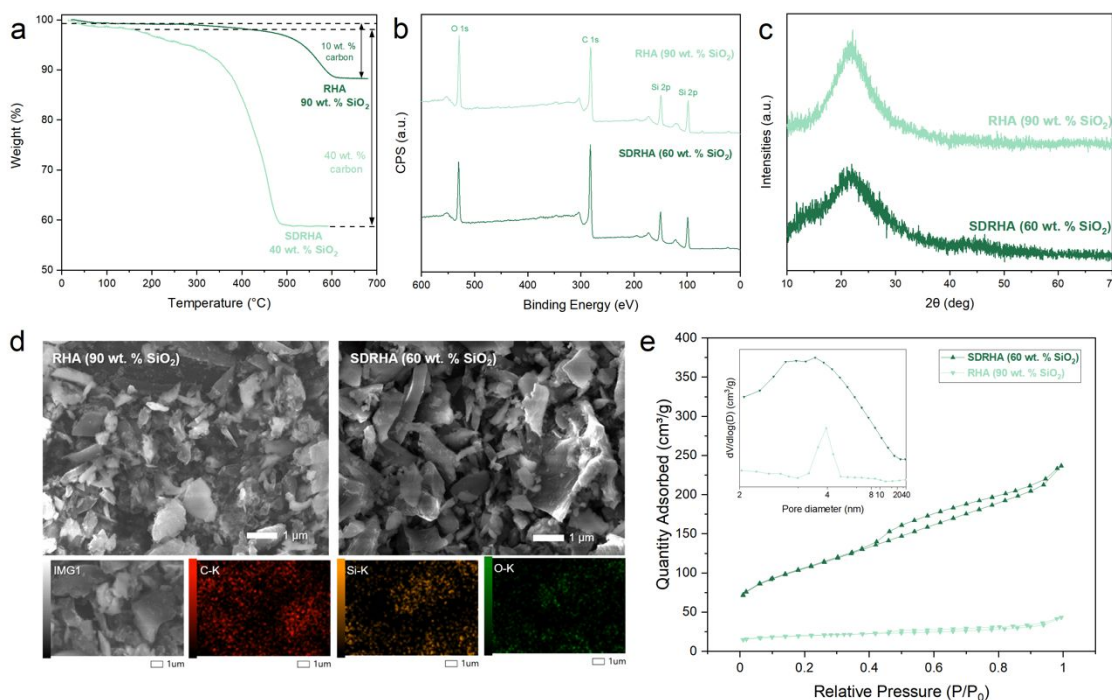


**Figure 1.** a. TGA, b. XPS survey scan, c. XRD, d. SEM images, and e. N<sub>2</sub> adsorption-desorption isothermal plots and pore size distribution (inset) of RHA and SDRHA<sub>60</sub>.

The SEM images (Figure 1d) reveal that RHA morphologies are retained in the SDRHA<sub>60</sub>, where the majority of particles range from 1 to 10  $\mu\text{m}$ . Moreover, the SiO<sub>2</sub> and carbon particles are mixed in a porous network, as visualized in the SEM images and

attested to by BET measurements. The BJH adsorption cumulative pore volume increases from  $\sim 0.05 \text{ cm}^3/\text{g}$  for RHA to  $\sim 0.3 \text{ cm}^3/\text{g}$  for SDRHA<sub>60</sub>. The pore size distributions in RHA and SDRHA<sub>60</sub> are illustrated in the inset of Figure 1e, where broader distributions of pores in the range of 2-4 nm are present in SDRHA<sub>60</sub>. The BET SSAs increase from  $\sim 70 \text{ m}^2/\text{g}$  for RHA to  $\sim 345 \text{ m}^2/\text{g}$  for SDRHA<sub>60</sub>, while those for SDRHA<sub>40,50,55,65</sub> are  $\sim 440$ ,  $\sim 420$ ,  $\sim 370$ , and  $\sim 220 \text{ m}^2/\text{g}$ . As seen in the N<sub>2</sub> adsorption-desorption isotherms of RHA and SDRHA<sub>60</sub>, the plot characteristics correspond to type IV with H3 hysteresis in IUPAC classifications, which presumably arises from the porous network in non-rigid aggregates of plate-like particles.<sup>47</sup> The enhanced pore volumes and SSAs likely facilitate interactions between SiO<sub>2</sub> and carbon particles and CO and SiO during carbothermal reductions.

#### Nanocomposites from SDRHA via carbothermal reduction

In traditional carbothermal reduction, it is necessary to mill the SiO<sub>2</sub> source with the carbon source as a first step. In contrast, SDRHA<sub>40-65</sub> consist of SiO<sub>2</sub>/C nanocomposites as recovered from distillative removal of SiO<sub>2</sub>. Thus, they can be heated directly. Figure 2a and Figure 2b present XRDs of SiC derived from heating SDRHA<sub>60</sub> at 1400-1500 °C under Ar for 8 h, and at 1500 °C for 2-7 h. The corresponding crystalline phases are listed in Table 1, determined using the reference intensity ratio method.

Peaks at 36°, 42°, 60°, and 72° 2θ are associated with the (111), (200), (220), and (311) planes of β-SiC (3C-SiC, PDF 01-073-1708). The weak shoulders at 33.5° correspond to stacking faults.<sup>48-50</sup> On heating to 1430 and 1450 °C, peaks indexed to the (101) plane of cristobalite at 22° 2θ appear, corresponding to  $\sim 20$  and 5 wt. % cristobalite

in the products, respectively. No cristobalite or other SiO<sub>2</sub> phase are observed for reaction times >5 h. Limiting heat-treatment to 4 h gives SiC as the major product with ~3 wt. % cristobalite.

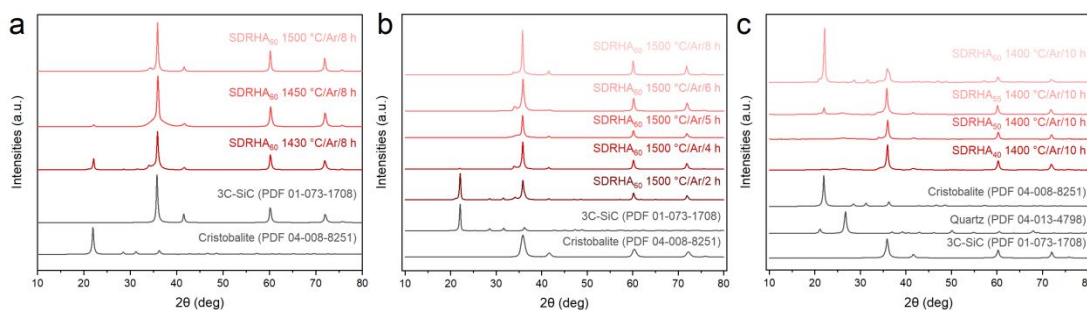


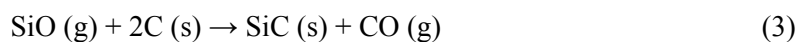
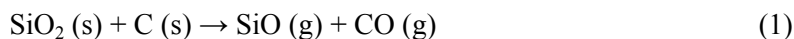
**Figure 2.** XRDs from heating **a.** SDRHA<sub>60</sub> at 1430-1500 °C/8 h/Ar, **b.** SDRHA<sub>60</sub> at 1500 °C for various times, **c.** SDRHA<sub>40-60</sub> at 1400 °C/10 h/Ar.

**Table 1.** Crystalline phases of products from heating SDRHA<sub>60</sub> at 1400-1500 °C/Ar.

SDRHA <sub>60</sub>	1430 °C/8 h	1450 °C/8 h	1500 °C/2 h	1500 °C/4 h	1500 °C/>5 h
SiC	80 %	95 %	57 %	98 %	100 %
Cristobalite	20 %	5 %	43 %	2 %	0 %

\*As-produced composites contain amorphous hard carbon (13.7 ± 0.9 wt. % of the total mass, determined by TGA)

Known reactions involved in the carbothermal reductive synthesis of SiC are:<sup>6,51,52</sup>



Previous studies proposed that temperatures lower than 1400 °C were unfavorable for carbothermal reduction and nitridation of RHA.<sup>33</sup> Possible explanations for this observation include rapid SiO<sub>2</sub> losses as gaseous SiO at temperatures ≤1400 °C and dominant solid-solid reactions occurred between SiO<sub>2</sub> and carbon particle contact points

(in micron scale mixtures) at temperatures  $\leq 1400$  °C.<sup>53–57</sup> Consequently, formation and coincident loss of CO suppresses further SiC formation. The effects of SiO<sub>2</sub>:C ratios are more critical for larger particle sizes.

Conventional carbothermal reduction requires excess carbon to promote complete transformation of SiO<sub>2</sub> to SiC.<sup>2,58,59</sup> The corresponding mole ratios of SiO<sub>2</sub>:C require greater carbon contents than a 1:3 stoichiometric ratio. SDRHA<sub>40,50,55,60</sub> materials offer SiO<sub>2</sub>:C mole ratios of 2:15, 1:5, 11:45, and 3:10, respectively, satisfying the excess carbon criterion.

As shown in Figure 2c, heating SDRHA<sub>40,50</sub> at 1400 °C for 10 h results in the formation of ~88 and 79 wt. % SiC, respectively, while SDRHA<sub>60</sub> gives ~16 wt. % (Table 2). The trend that more carbon in the starting materials leads to a higher proportion of SiC in the products agrees with studies reported earlier that surplus carbon facilitates increases in SiC yields. It is also in keeping with reaction kinetics, wherein higher concentrations of a given reactant will drive a given reaction faster.

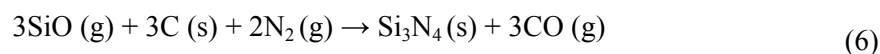
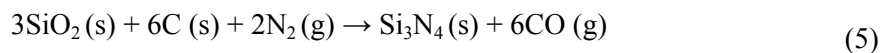
The detection of two crystalline SiO<sub>2</sub> phases in products heated at 1400 °C suggests incomplete transformation from quartz to cristobalite, which is reported to occur over the temperature interval of 1100–1400 °C.<sup>60–62</sup> In addition, it is well known that carbon reduces SiO<sub>2</sub> to SiO; thereby initiating vapor-vapor reactions between SiO and C/CO rather than solid-state reactions alone and leads to lower SiC formation temperatures.<sup>63</sup> All these factors define the trend shown in Table 2, where higher SiC yields result from higher initial carbon contents. The residual hard carbon is easily removed oxidatively at 600 °C or can be part of an SiC/C anode in lithium ion batteries, as will be reported at a later date.

**Table 2.** Phase compositions of products from heating SDRHA<sub>40-60</sub> at 1400 °C/10 h/Ar.

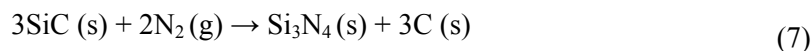
1400 °C/Ar/10 h				
Starting material	SDRHA <sub>40</sub>	SDRHA <sub>50</sub>	SDRHA <sub>55</sub>	SDRHA <sub>60</sub>
SiC	88 %	79 %	74 %	16 %
Cristobalite	3 %	2 %	7 %	82 %
Quartz	9 %	19 %	20 %	2 %
Amorphous carbon*	34 %	22 %	20 %	10 %

\*Amorphous hard carbon contents are out of the total mass of the as-produced (determined by TGA)

XRD analyses of SDRHA<sub>60</sub> heated under N<sub>2</sub> confirm formation of  $\alpha$ -Si<sub>3</sub>N<sub>4</sub> (Figure **3a** and **b**) per:



No significant peak attributable to SiO<sub>2</sub> or SiC is observed, as commonly found in Si<sub>3</sub>N<sub>4</sub> produced by carbothermal nitridation, indicating complete nitridation of SiO<sub>2</sub> under the conditions employed.<sup>29,31</sup> Meanwhile, SiO<sub>2</sub>:C ratios significantly impact the reaction. SDRHA<sub>60</sub> provides a mole ratio higher than the stoichiometric SiO<sub>2</sub>:C ratio of 1:2 for carbonitriding of SiO<sub>2</sub>, resulting in ~24 wt. % residual carbon in the products, as discussed below. XRDs in Figure **3b** indicate that products derived from SDRHA<sub>65</sub> (SiO<sub>2</sub>:C mole ratio = 13:35) consist of Si<sub>3</sub>N<sub>4</sub>, Si<sub>2</sub>N<sub>2</sub>O, SiC, and cristobalite (Table **3**) as well as residual hard carbon. The relative Si<sub>3</sub>N<sub>4</sub> and SiC compositions correlate with the secondary reaction:



Peak intensities indexed to cristobalite at  $22^\circ$   $2\theta$  decrease at longer heating times, becoming negligible after 8 h.

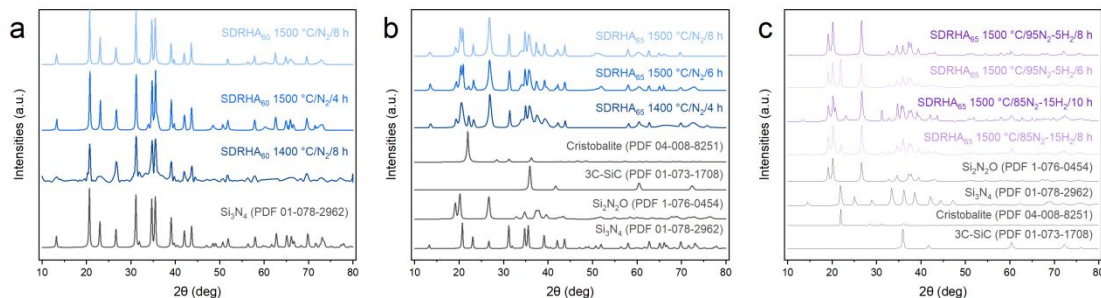


**Figure 3.** XRDs from heating **a.** SDRHA<sub>60</sub> at 1400/8 h/N<sub>2</sub>, 1500 °C/4 h/N<sub>2</sub>, 1500 °C/8 h/N<sub>2</sub>, SDRHA<sub>65</sub> at 1500 °C under **b.** N<sub>2</sub> and **c.** N<sub>2</sub>-H<sub>2</sub> with different ratios (95-5 and 85-15) for various times.

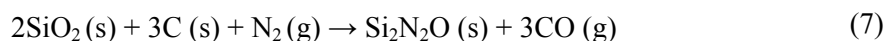
Silicon oxynitride (Si<sub>2</sub>N<sub>2</sub>O), a refractory material with high chemical and oxidation resistance, is a non-negligible phase produced during carbothermal nitridation SDRHA<sub>65</sub>. Gundiah *et al.*<sup>64</sup> obtained Si<sub>2</sub>N<sub>2</sub>O nanowires (dia. ~300 nm) by reacting silica gel with carbon nanotubes at 1360 °C/4 h/NH<sub>3</sub>, while longer treatments ( $\geq 7$  h) generated mainly Si<sub>3</sub>N<sub>4</sub> nanowires. Ramesh *et al.*<sup>65</sup> reported that carbothermal reduction and nitridation of amorphous SiO<sub>1.7</sub> at 1623 K (1350 °C) lead exclusively to formation of Si<sub>2</sub>N<sub>2</sub>O and reactions of amorphous SiO<sub>2</sub> lead exclusively to the formation of Si<sub>3</sub>N<sub>4</sub>. Ma *et al.*<sup>66</sup> successfully synthesized Si<sub>2</sub>N<sub>2</sub>O powders using diatomite and sucrose as silicon and carbon sources via carbothermal nitridation with a SiO<sub>2</sub>:C molar ratio of 2 and a temperature of 1550 °C as the optimized parameters. Multiple other groups also report increasing yields of Si<sub>2</sub>N<sub>2</sub>O on adding catalysts: Y<sub>2</sub>O<sub>3</sub>,<sup>67,68</sup> Fe,<sup>64</sup> and Fe<sub>2</sub>O<sub>3</sub><sup>69</sup> into mixtures of SiO<sub>2</sub> and carbon. Such catalytic additives can become impurities in the products.

**Table 3.** Crystalline phase compositions from heating SDRHA<sub>65</sub> at 1500 °C for various times under N<sub>2</sub> or N<sub>2</sub>-H<sub>2</sub> with different ratios (95/5 and 85/15).

SDRHA <sub>65</sub>							
Temperature	1500 °C						
Atmosphere	N <sub>2</sub>			95N <sub>2</sub> -5H <sub>2</sub>		85N <sub>2</sub> -15H <sub>2</sub>	
Duration	4 h	6 h	8 h	6 h	8 h	8 h	10 h
Si <sub>2</sub> N <sub>2</sub> O	32%	33%	36%	74%	84%	70%	88%
Si <sub>3</sub> N <sub>4</sub>	38%	50%	58%	5%	<1%	12%	5%
SiC	26%	15%	36%	2%	6%	14%	2%
Cristobalite	4%	2%	6%	19%	<1%	4%	5%
Amorphous carbon*	15.3 ± 1.1 %			5.7 ± 0.9 %			

\*Amorphous hard carbon contents from total mass of as-produced material (determined by TGA).

Interestingly, composites with Si<sub>2</sub>N<sub>2</sub>O as the major phase (>70 wt. % of the total mass) were produced by heating SDRHA in an N<sub>2</sub>:H<sub>2</sub> mixture. Theoretically, the stoichiometric SiO<sub>2</sub>:C mole ratio is 2:3, per:



SDRHA<sub>65</sub>, with a relatively higher SiO<sub>2</sub>:C mole ratio (13:35), was chosen to access sufficient oxygen from SiO<sub>2</sub>, by which composites with relatively low excess carbon (5.7 ± 0.9 wt. %) were obtained. Figure 3c illustrates representative XRDs of product phases from heating SDRHA<sub>65</sub> in N<sub>2</sub>:H<sub>2</sub> at 95N<sub>2</sub>:5H<sub>2</sub> or 85N<sub>2</sub>:15H<sub>2</sub>. Similar to the aforementioned Si<sub>3</sub>N<sub>4</sub> products, Si<sub>2</sub>N<sub>2</sub>O, Si<sub>3</sub>N<sub>4</sub>, SiC, and cristobalite phases are present in the composites (Table 3). With longer heating times, further reduction leads to higher conversions reducing cristobalite content but coincidentally generating more Si<sub>3</sub>N<sub>4</sub>, as

prolonged treatment times will result in further reduction of oxygen in  $\text{Si}_2\text{N}_2\text{O}$ , forming  $\text{Si}_3\text{N}_4$ :



Addition of  $\text{H}_2$  in the systems leads to lower  $\text{N}_2$  partial pressures and consequently lower  $\text{Si}_3\text{N}_4$  yields,<sup>70</sup> while the presence of  $\text{H}_2$  affects the carbonitriding mechanisms by both direct and indirect reduction of  $\text{SiO}_2$  per:

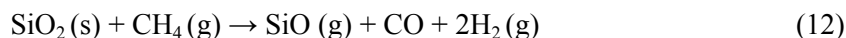
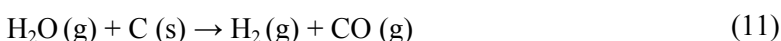
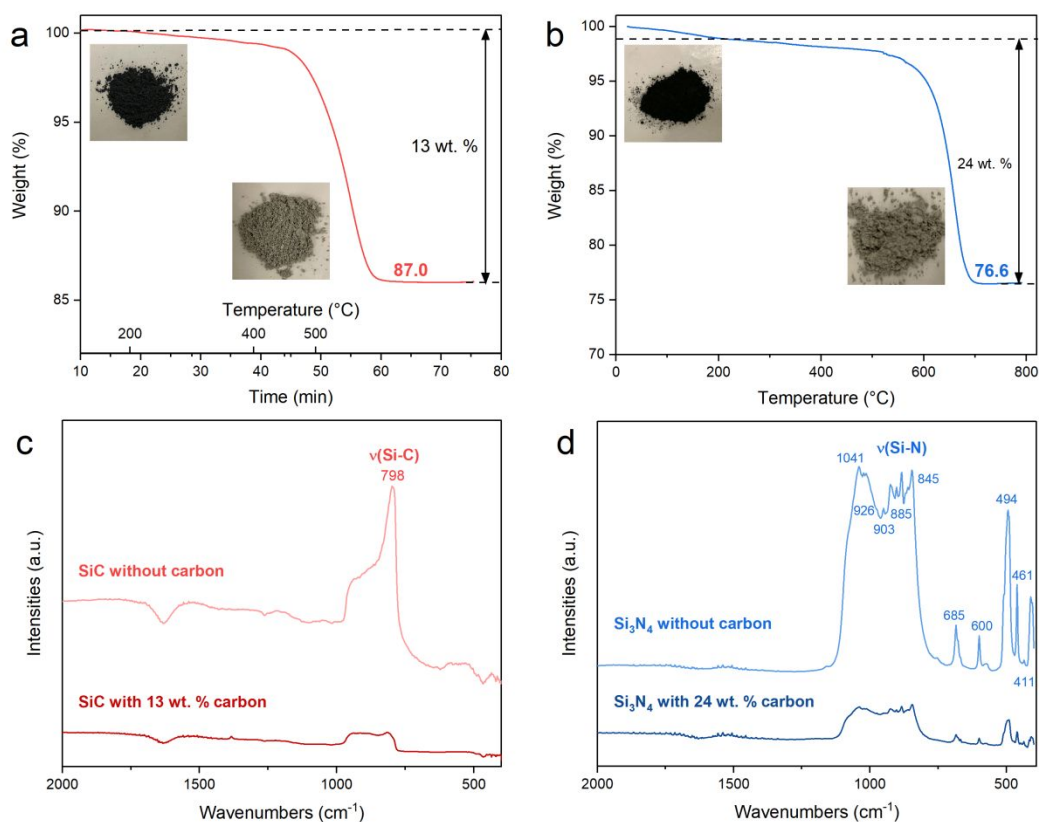


Figure **4a** and **b** illustrate TGAs of representative products derived from carbothermal reduction of SDRHA with SiC and  $\text{Si}_3\text{N}_4$  as the major phase, indicating excess carbon remains in all systems when heated to 1500 °C. Thus, ~13 wt. % unreacted carbon remains in SiC, whereas as-produced  $\text{Si}_3\text{N}_4$  retains ~24 wt. % carbon. The resulting composite powders appear as dark grey due to mixed with excess carbon, which shows light grey green after oxidative removal of residual carbon, the typical color of SiC and  $\text{Si}_3\text{N}_4$  produced in conventional manufacturing. Given that less carbon is involved in the starting SDRHA<sub>65</sub> for synthesizing  $\text{Si}_2\text{N}_2\text{O}$  and more carbon is consumed by reacting with  $\text{H}_2$ , a lower amount of excess carbon is found in the composites ( $5.7 \pm 0.9$  wt. %) than in the former two systems.



**Figure 4.** Representative TGA curves and optical images of **a.** SiC, **b.** Si<sub>3</sub>N<sub>4</sub>, and FTIR spectra of **c.** SiC, **d.** Si<sub>3</sub>N<sub>4</sub> composites with and without carbon.

The Figure 4c FTIR of SiC with 13 wt. % carbon presents a broad peak from 790 to 1000 cm<sup>-1</sup> corresponding to the overlap of v(Si-C) and v(C-C). After oxidation at 500 °C/O<sub>2</sub>/1 h, a strong absorption appears centered at 798 cm<sup>-1</sup> that can be assigned to v(Si-C), suggesting the formation of cubic SiC,<sup>71</sup> consistent with the β-SiC phase indexed from XRD results discussed above. The enhanced intensity of v(Si-C) peak at ~800 cm<sup>-1</sup> is presumably due to exposure of SiC after removing the excess carbon.

In the spectrum of Si<sub>3</sub>N<sub>4</sub> (Figure 4d), the broad band from 800 to 1100 cm<sup>-1</sup> reveals an overlap of v(Si-N) and v(Si-O) from components including Si<sub>3</sub>N<sub>4</sub> and SiO<sub>2</sub> from oxidation of Si<sub>3</sub>N<sub>4</sub> particle surfaces.<sup>32</sup> Similar to the SiC product, peak intensities are

enhanced on removing excess carbon. The bands at 926, 903, 885, 845, and 685  $\text{cm}^{-1}$  are typical for  $\alpha\text{-Si}_3\text{N}_4$ , compatible with XRD results.

In composites with  $\text{Si}_2\text{N}_2\text{O}$  as the major phase, the characteristic peaks of  $\text{Si}_2\text{N}_2\text{O}$  at 1090, 989, 910, and 679  $\text{cm}^{-1}$  are observed (Figure 5a).<sup>72</sup> An additional band at 850  $\text{cm}^{-1}$  is shown in the composites from heating  $\text{SDRHA}_{65}$  at 1500  $^\circ\text{C}/6\text{ h}/95\text{N}_2\text{-}5\text{H}_2$ , which is attributed to  $\nu(\text{Si-C})$  and  $\nu(\text{Si-O})$  from SiC and cristobalite phases in the system.

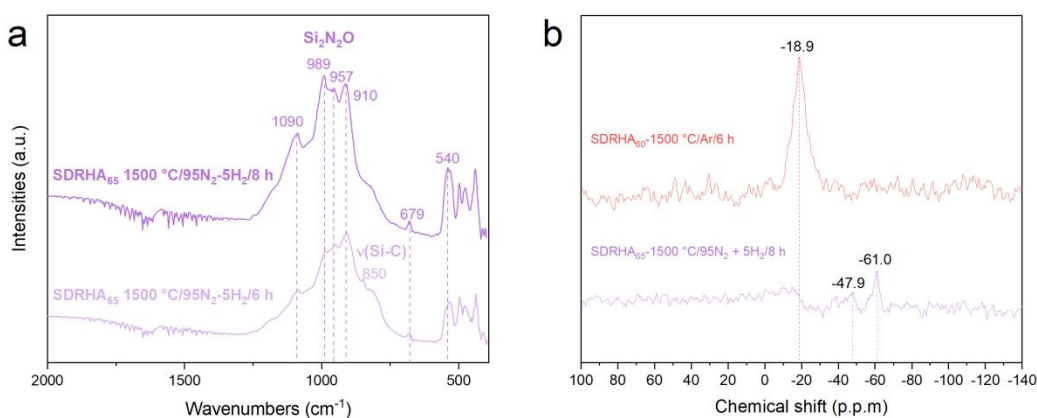


**Figure 5.** Representative **a.** FTIR spectra of  $\text{Si}_2\text{N}_2\text{O}$  composites from different heat treatments, and **b.**  $^{29}\text{Si}$  NMR of SiC and  $\text{Si}_2\text{N}_2\text{O}$  composites.

Figure 5b presents solid-state  $^{29}\text{Si}$  NMR spectra of representative SiC and  $\text{Si}_2\text{N}_2\text{O}$  composites derived from SDRHA. The  $^{29}\text{Si}$  chemical shift is sensitive to adjacent bonded atoms; thus, small differences in the various polymorphs of one compound can be resolved. The single resonance peak centered at  $\sim -19$  ppm is associated with  $\text{SiC}_4$  units in  $\beta\text{-SiC}$ , consistent with the XRD discussed above (Figure 2).<sup>73–75</sup> Typically, broader line widths in solid-state NMR spectra are associated with samples of lower crystallinity. The relatively broad peak width is ascribed to some extent to crystalline disorder (e.g.

twinning, stacking faults), as confirmed by the weak shoulder at  $\sim 34^\circ 2\theta$  indexed to stacking faults.

As for the  $\text{Si}_2\text{N}_2\text{O}$  composites from carbonitridation, the  $^{29}\text{Si}$  resonance at  $\sim -61$  ppm corresponds to the tetrahedral  $\text{SiN}_3\text{O}$  structural unit in  $\text{Si}_2\text{N}_2\text{O}$ .<sup>74</sup> The  $^{29}\text{Si}$  resonance peak at  $\sim -48$  ppm is assigned to tetrahedral Si-N in  $\text{Si}_3\text{N}_4$ ,<sup>74</sup> while the weak hump at  $\sim -19$  ppm probably arises from nanocrystalline SiC, as identified by XRD. However, no peak associated with cristobalite ( $\sim -110$  ppm<sup>76,77</sup>) is observed in the spectrum, presumably due to its low content in the sample.

XPS was used to identify the elemental compositions and oxidation states of products with SiC,  $\text{Si}_3\text{N}_4$ , and  $\text{Si}_2\text{N}_2\text{O}$  as the major phase. The survey scans of all composites show signature peaks associated with corresponding elements, where no impurities are detected (Figure S1). The representative XPS spectra shown in Figure 6a and Figure S2 correspond to products from SDRHA<sub>60</sub> heated at 1500 °C/8 h before and after oxidative removal of carbon, respectively. Both of the Si 2s and Si 2p spectra in Figure S2 exhibit one single peak associated with the  $\text{Si}^{4+}$  state in SiC composites.<sup>78-80</sup>

Deconvolution of the Si 2p region reveals peaks at 101.7 eV for Si-C bonds, while a second peak at 102.5 eV originates from the incorporation of oxygen, resulting in a shift to higher binding energy. In comparison, the Si 2p double peaks at  $\sim 101$  and  $\sim 103.1$  eV for Si-C and Si-O bonds, respectively, are observed in the spectra collected from the SiC sample following oxidative removal of carbon.<sup>81,82</sup> The most easily oxidized SiC surface, the SiC whiskers most likely provide the distinct Si-O peaks derived from surface oxidation during oxidative removal of carbon.<sup>79</sup> The C 1s spectra of SiC before and after removing carbon are both fitted with four Gaussian peaks, while the peak at  $\sim 283.5$  eV

indexed to Si-C bonds is more evident in spectra taken after removal of carbon. Intense peaks ascribed to C-C bonds (285.2 - 285.6 eV), and two other components associated with C-O (287.1 eV) and C=O bonds (289.5 eV) originate from the residual hard carbon.<sup>83,84</sup>

As for the  $\text{Si}_3\text{N}_4$ , from heating  $\text{SDRHA}_{60}$  at 1500 °C/8 h/ $\text{N}_2$  (Figure 6b), peak fitting in the Si 2p region reveals an intense peak at 101.8 eV attributed to  $\text{Si}_3\text{N}_4$ .<sup>82</sup> The component at 102.8 eV is assigned to Si-O bonds when the Si atoms bonded to both N and O, as the Si-O bonds originate from oxidation during carbon removal. The intense peak located at 398.1 eV in the N 1s spectra is assigned to N-Si bonds in  $\text{Si}_3\text{N}_4$ , while N-O bonds correspond to the weak peak at 399.4 eV.<sup>85-87</sup>

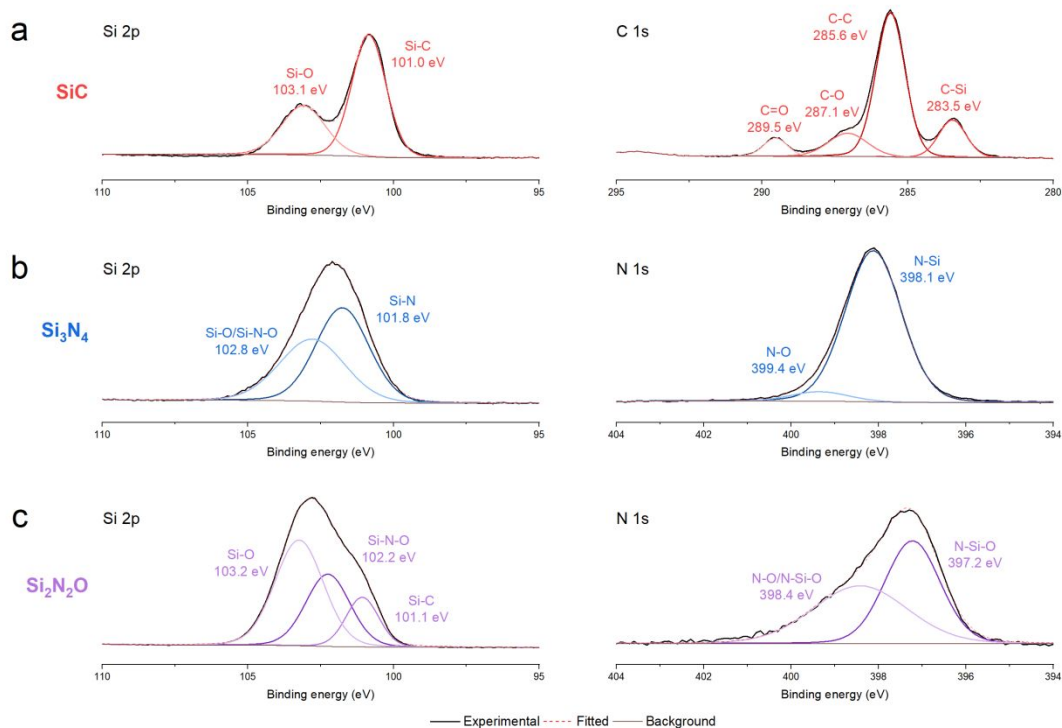


**Figure 6.** Representative XPS core-level spectra of **a.** SiC, **b.**  $\text{Si}_3\text{N}_4$ , and **c.**  $\text{Si}_2\text{N}_2\text{O}$  composites.

In comparison, the Si 2p spectra of the  $\text{Si}_2\text{N}_2\text{O}$  composite (SDRHA<sub>65</sub>-1500 °C/8 h/95N<sub>2</sub>-5H<sub>2</sub>) shown in Figure 6c consist of three fitted peaks. The two peaks located at 103.2 eV and 102.2 eV are attributed to Si-O and Si-N-O bonds,<sup>88,89</sup> respectively, where the shifts compared to Si-O bonds in  $\text{SiO}_2$  and Si-N bonds in  $\text{Si}_3\text{N}_4$  are typical for  $\text{Si}_2\text{N}_2\text{O}$ .<sup>90</sup> Si-C bonds of SiC in the composites show another peak at 101.1 eV, consistent with analyses from XRD. Meanwhile, peaks at 398.4 eV and 397.2 eV in the N 1s spectra can be assigned to N-Si-O bonds and N-O bonds within the  $\text{Si}_2\text{N}_2\text{O}$  structure.

SEM and EDX images in Figure 7 were obtained from the oxidized samples, revealing cylindrical morphologies. SiC particles with sizes ranging between 10 and 200 nm can be observed among SiC whiskers with diameters of 100-140 nm and lengths up to 5  $\mu\text{m}$ . EDS maps show well-distributed Si and C elements. Oxygen was also detected after oxidative carbon removal, as discussed above.

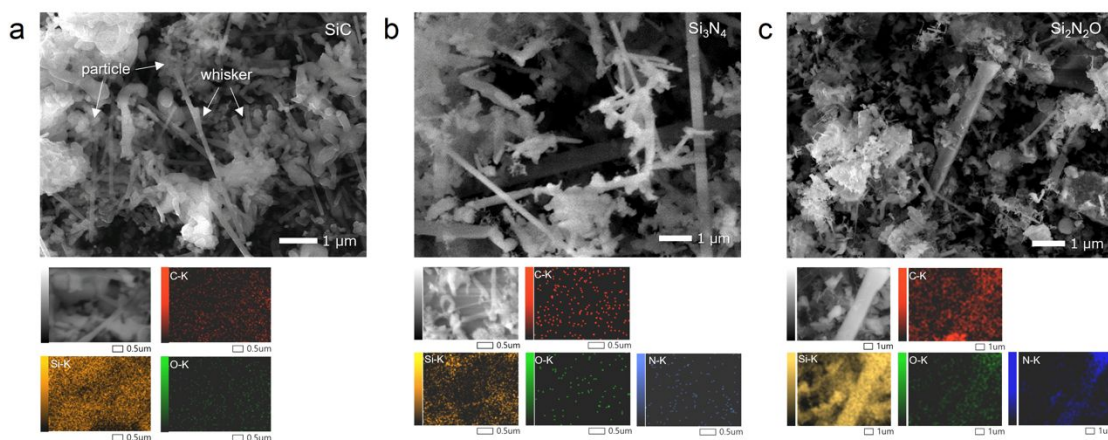


**Figure 7.** Representative SEM and EDX images of **a.** SiC, **b.**  $\text{Si}_3\text{N}_4$ , and **c.**  $\text{Si}_2\text{N}_2\text{O}$  composites.

The proposed SiC whisker growth mechanisms focus on heterogeneous vapor-liquid-solid, birth-and-spread growth, vapor-vapor growth.<sup>91,92</sup> Nucleation and growth of SiC

whiskers are believed to result mainly from gas-phase reactions between SiO and CO.<sup>93</sup> Although the formation and growth of SiC polymorphs are not fully understood as yet, it is widely accepted that additives, starting materials, impurities, and growth conditions all affect the crystallization kinetics of SiC and the subsequent differences in polymorphs and phases.<sup>10,93,94</sup> Similar morphologies are observed in the Si<sub>3</sub>N<sub>4</sub> and Si<sub>2</sub>N<sub>2</sub>O composites (Figure 7b and c). Irregular aggregates mixed with whiskers with diameters of 100-200 nm predominate and are several microns in length.

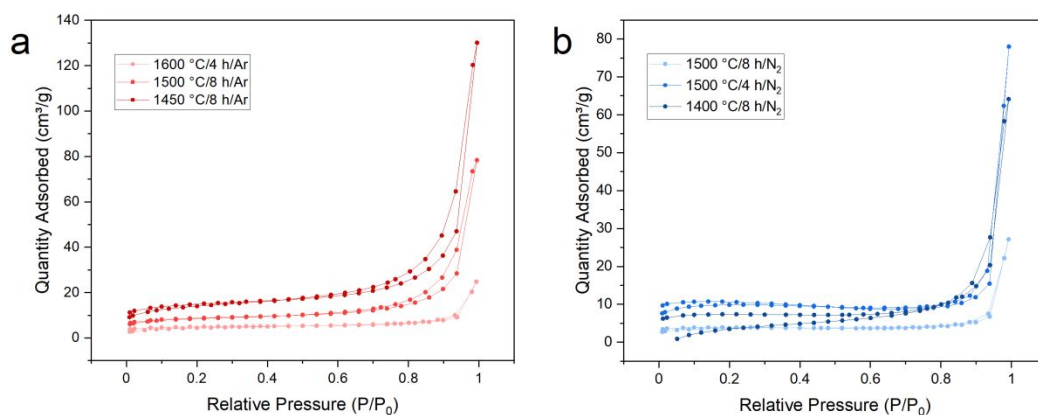


**Figure 8.** Representative N<sub>2</sub> adsorption-desorption isotherm plots of **a.** SiC and **b.** Si<sub>3</sub>N<sub>4</sub>.

The as-synthesized composites show BET SSAs of >150 m<sup>2</sup>/g with excess hard carbon. Oxidative removal of carbon followed by BET studies were undertaken, by which the N<sub>2</sub> adsorption isotherms for SiC and Si<sub>3</sub>N<sub>4</sub> obtained on heating at different temperatures are depicted in Figure 8a and b. Incremental increases in the measured BET SSAs were observed with lower synthesis temperatures. The BET surface areas of SiC from heating at 1450, 1500, and 1600 °C for 8 h are 44, 27, and 10 m<sup>2</sup>/g, respectively.

BET studies of Si<sub>3</sub>N<sub>4</sub> from heating SDRHA<sub>60</sub> at 1400 and 1500 °C/8 h/N<sub>2</sub> reveal surface areas of ~20 and ~10 m<sup>2</sup>/g, respectively. In comparison, Si<sub>3</sub>N<sub>4</sub> produced from

heating at 1500 °C/4 h shows an SSA of ~30 m<sup>2</sup>/g; while Si<sub>2</sub>N<sub>2</sub>O from heating SDRHA<sub>65</sub> at 1500 °C/8 h/95N<sub>2</sub>-5H<sub>2</sub> show SSAs of ~10 m<sup>2</sup>/g. As expected, higher and longer heating temperatures and times result in decreases in specific surface areas, presumably due to the growth and coalescence of fibers and particulates via grain-boundary diffusion.<sup>91,95</sup>

The aforementioned studies on composites derived from SDRHA are preludes to investigations using these materials as compatible components in Li<sup>+</sup> energy storage devices. As available free surfaces are believed to correlate with charge/discharge kinetics and reversibility, composites with optimized SSAs and appropriate modifications of residual hard carbon contents are in progress.<sup>83,96–100</sup>

## Conclusions

SDRHA with adjustable SiO<sub>2</sub>:C ratios makes it an attractive starting material for synthesizing SiC, Si<sub>3</sub>N<sub>4</sub>, and Si<sub>2</sub>N<sub>2</sub>O whisker and particle composites. Complete conversion of the SiO<sub>2</sub> in SDRHA to β-SiC was evidenced in samples heated at 1500 °C/5 h/Ar, while that for α-Si<sub>3</sub>N<sub>4</sub> is 1400 °C/8 h/N<sub>2</sub>. On heating under N<sub>2</sub>-H<sub>2</sub> mixtures, Si<sub>2</sub>N<sub>2</sub>O forms as the major crystalline phase (up to 88 wt. %). Higher temperatures and longer reaction times enhance SiO<sub>2</sub> reduction but at the expense of BET SSAs, which are desirable for electronic applications and for use in lithium battery applications as will be described in a forthcoming paper.

Likewise, lower SiO<sub>2</sub>:C ratios in SDRHA, *i.e.* more excess carbon in the starting materials facilitate carbothermal reduction at lower temperatures. Amounts of excess free carbon contained in all product composites vary with the SiO<sub>2</sub>:C ratio in the starting SDRHA and heating conditions and can be easily eliminated oxidatively. The absence of

metal impurities in the products derived from SDRHA overcomes the long-lasting challenges of generating products with high purities from agricultural wastes, enabling their potential used in various applications.

### **Conflicts of interest**

There are no conflicts to declare.

### **Acknowledgments**

We acknowledge DMR NSF Grant No. DMR-1926199 and a generous gift from Mercedes Benz Research and Development North America (MBRDNA) as support for this work. We also thank the gift of RHA from Wadham Energy Inc., the technical support provided by Michigan Center for Materials Characterization, and Zijing Zhang for the help in studies on  $\text{Si}_2\text{N}_2\text{O}$  composites.

### REFERENCES

- 1 S. S. Hossain, L. Mathur and P. K. Roy, *Journal of Asian Ceramic Societies*, 2018, **6**, 299–313.
- 2 J. G. Lee, P. D. Miller and I. B. Cutler, in *Reactivity of Solids*, eds. J. Wood, O. Lindqvist, C. Helgesson and N.-G. Vannerberg, Springer US, Boston, MA, 1977, pp. 707–711.
- 3 W.-S. Seo, K. Koumoto and S. Aria, *Journal of the American Ceramic Society*, 2000, **83**, 2584–2592.
- 4 M. F. Zawrah, M. A. Zayed and M. R. K. Ali, *Journal of Hazardous Materials*, 2012, **227–228**, 250–256.

- 5 R. Rajarao and V. Sahajwalla, *Journal of Cleaner Production*, 2016, **133**, 1277–1282.
- 6 Y. L. Chiew and K. Y. Cheong, *Materials Science and Engineering: B*, 2011, **176**, 951–964.
- 7 A. Selvam, N. G. Nair and P. Singh, *Journal of Materials Science Letters*, 1998, **17**, 57–60.
- 8 S. Maroufi, M. Mayyas and V. Sahajwalla, *ACS Sustainable Chem. Eng.*, 2017, **5**, 4171–4178.
- 9 S. Maroufi, M. Mayyas and V. Sahajwalla, *Journal of Cleaner Production*, 2017, **157**, 213–221.
- 10 F. J. Narciso-Romero and F. Rodríguez-Reinoso, *JOURNAL OF MATERIALS SCIENCE*, 1996, **31**, 779–784.
- 11 J. Kuang and W. Cao, *Journal of the American Ceramic Society*, 2013, **96**, 2877–2880.
- 12 S.-C. Chiu, H.-C. Yu and Y.-Y. Li, *J. Phys. Chem. C*, 2010, **114**, 1947–1952.
- 13 C. Real, M. D. Alcalá and J. M. Criado, *Journal of the American Ceramic Society*, 2004, **87**, 75–78.
- 14 R. Pode, *Renewable and Sustainable Energy Reviews*, 2016, **53**, 1468–1485.
- 15 Y. Shen, P. Zhao and Q. Shao, *Microporous and Mesoporous Materials*, 2014, **188**, 46–76.
- 16 M. M. Haslinawati, K. A. Matori, Z. A. Wahab, H. A. A. Sidek and A. T. Zainal, 2009, **09**, 4.
- 17 J. Su, B. Gao, Z. Chen, J. Fu, W. An, X. Peng, X. Zhang, L. Wang, K. Huo and P. K. Chu, *ACS Sustainable Chem. Eng.*, 2016, **4**, 6600–6607.
- 18 J. Li, T. Shirai and M. Fuji, *Journal of the Ceramic Society of Japan*, 2012, **120**, 338–340.
- 19 P. Gorthy and M. P. G, *Journal of the American Ceramic Society*, 1999, **82**, 1393–1400.
- 20 K. Sujirote and P. Leangsuwan, *Journal of Materials Science*, 2003, **38**, 4739–4744.
- 21 Y. Zou and T. Yang, in *Rice Bran and Rice Bran Oil*, eds. L.-Z. Cheong and X. Xu, AOCS Press, 2019, pp. 207–246.
- 22 B. Singh, in *Waste and Supplementary Cementitious Materials in Concrete*, eds. R. Siddique and P. Cachim, Woodhead Publishing, 2018, pp. 417–460.

- 23 M. A. Hamad and I. A. Khattab, *Thermochimica Acta*, 1981, **48**, 343–349.
- 24 V. Vaibhav, U. Vijayalakshmi and S. M. Roopan, *Spectrochimica Acta Part A: Molecular and Biomolecular Spectroscopy*, 2015, **139**, 515–520.
- 25 A. Yeoh and R. Biden, in *Proceedings of UNIDO/ESCAP/ RCTT*, Alor Setar, Malaysia.
- 26 C. Hwang and D. Wu, *American Concrete Institute SP*, 733–765.
- 27 W. Li, Q. Huang, H. Guo and Y. Hou, *Ceramics International*, 2018, **44**, 4500–4503.
- 28 J. Chen, Q. Kong, Z. Liu, Z. Bi, H. Jia, G. Song, L. Xie, S. Zhang and C.-M. Chen, *ACS Sustainable Chem. Eng.*, 2019, **7**, 19027–19033.
- 29 A. Ortega, M. D. Alcalá and C. Real, *Journal of Materials Processing Technology*, 2008, **195**, 224–231.
- 30 N. Wangmooklang, K. Sujirote, S. Jinawath and S. Wada, *Journal of the European Ceramic Society*, 2007, **27**, 2111–2117.
- 31 X. Wan, The Univerdity of New South Wales.
- 32 A. Abdulhameed, H. Mbuvi and E. O. Changamu, , DOI:10.31021/JWT.20181106.
- 33 V. Pavarajarn, R. Precharyutasin and P. Prasertthdam, *Journal of the American Ceramic Society*, 2010, **93**, 973–979.
- 34 R. V. Krishnarao and M. M. Godkhindi, *Ceramics International*, 1992, **18**, 243–249.
- 35 J. C. Marchal, D. J. Krug, P. McDonnell, K. Sun and R. M. Laine, *Green Chemistry*, 2015, **17**, 3931–3940.
- 36 X. Ma, B. Zhou, W. Gao, Y. Qu, L. Wang, Z. Wang and Y. Zhu, *Powder Technology*, 2012, **217**, 497–501.
- 37 U. Kalapathy, A. Proctor and J. Shultz, *Bioresource Technology*, 2000, **73**, 257–262.
- 38 R. M. Laine, J. C. Furgal, P. Doan, D. Pan, V. Popova and X. Zhang, *Angewandte Chemie*, 2016, **128**, 1077–1081.
- 39 X. Zhang, E. Temeche and R. M. Laine, *Green Chem.*, 2020, **22**, 7491–7505.
- 40 C. D. Li, M. U. Saeed, N. Pan, Z. F. Chen and T. Z. Xu, *Materials and Design*, , DOI:10.1016/j.matdes.2016.06.071.
- 41 E. Temeche, M. Yu and R. M. Laine, *Green Chem.*, 2020, **22**, 4656–4668.
- 42 R. M. Laine, J. C. Furgal, P. Doan, D. Pan, V. Popova and X. Zhang, *Angewandte Chemie International Edition*, 2016, **55**, 1065–1069.

- 43 Karnowo, Z. F. Zahara, S. Kudo, K. Norinaga and J. I. Hayashi, *Energy and Fuels*, 2014, **28**, 6459–6466.
- 44 A. Chakraverty, P. Mishra and H. D. Banerjee, *J Mater Sci*, 1988, **23**, 21–24.
- 45 B. K. Padhi and C. Patnaik, *Ceramics International*, 1995, **21**, 213–220.
- 46 G. Ayalasomayajuala, A. Garg, S. Kapila, K. Chandrashekhara and V. Flanigan, *International SAMPE Technical Conference*, 2004, 2435–2444.
- 47 M. Thommes, K. Kaneko, A. V. Neimark, J. P. Olivier, F. Rodriguez-Reinoso, J. Rouquerol and K. S. W. Sing, *Pure and Applied Chemistry*, 2015, **87**, 1051–1069.
- 48 A. L. Ortiz, F. Sánchez-Bajo, F. L. Cumbreira and F. Guiberteau, *Materials Letters*, 2001, **49**, 137–145.
- 49 G. Luo, Z. Zhang, J. Hu, J. Zhang, Y. Sun, Q. Shen and L. Zhang, *Materials*, 2020, **13**, 1496.
- 50 Y. Cui, J. Chen, Y. Di, X. Zhang and W. Lei, *AIP Advances*, 2017, **7**, 125219.
- 51 J.-G. Lee and I. B. Cutler, *American Ceramic Society Bulletin*, 1975, **54**, 195–198.
- 52 B. V. Radhakrishna Bhat and G. P. Sanghi, *Bull. Mater. Sci.*, 1987, **9**, 295–303.
- 53 J. L. Blumenthal, M. J. Santy and E. A. Burns, *AIAA Journal*, 1966, **4**, 1053–1057.
- 54 C. Y. Chen, C. I. Lin and S. H. Chen, *British Ceramic Transactions*, 2000, **99**, 57–62.
- 55 A. W. Weimer, K. J. Nilsen, G. A. Cochran and R. P. Roach, *AIChE Journal*, 1993, **39**, 493–503.
- 56 V. D. Krstic, *Journal of the American Ceramic Society*, 1992, **75**, 170–174.
- 57 N. Klinger, E. L. Strauss and K. L. Komarek, *Journal of the American Ceramic Society*, 1966, **49**, 369–375.
- 58 P. D. Miller, J. G. Lee and I. B. Cutler, *Journal of the American Ceramic Society*, 1979, **62**, 147–149.
- 59 A. Taylor and D. S. Laidler, *Br. J. Appl. Phys.*, 1950, **1**, 174–181.
- 60 K. F. Jusnes, M. Tangstad and E. Ringdalen, in *Extraction 2018*, eds. B. R. Davis, M. S. Moats, S. Wang, D. Gregurek, J. Kapusta, T. P. Battle, M. E. Schlesinger, G. R. Alvear Flores, E. Jak, G. Goodall, M. L. Free, E. Asselin, A. Chagnes, D. Dreisinger, M. Jeffrey, J. Lee, G. Miller, J. Petersen, V. S. T. Ciminelli, Q. Xu, R. Molnar, J. Adams, W. Liu, N. Verbaan, J. Goode, I. M. London, G. Azimi, A. Forstner, R. Kappes and T. Bhambhani, Springer International Publishing, Cham, 2018, pp. 717–727.

- 61 S. s Cole, *Journal of the American Ceramic Society*, 1935, **18**, 149–154.
- 62 A. C. D. Chaklader and A. L. Roberts, *Journal of the American Ceramic Society*, 1961, **44**, 35–41.
- 63 J. Li, T. Shirai and M. Fuji, *Advanced Powder Technology*, 2013, **24**, 838–843.
- 64 G. Gundiah, G. V. Madhav, A. Govindaraj, M. M. Seikh and C. N. R. Rao, *J. Mater. Chem.*, 2002, **12**, 1606–1611.
- 65 P. D. Ramesh and K. J. Rao, *Journal of Materials Research*, 1994, **9**, 2330–2340.
- 66 B. Ma, Z. Huang, L. Mei, M. Fang, Y. Liu, X. Wu and X. Hu, *JOM*, 2016, **68**, 1456–1464.
- 67 S. W. Yang, S. Y. Shan, W. H. Ma and H. Wang, *Materials Science Forum*, 2011, **675–677**, 175–178.
- 68 B. Bergman and H. Heping, *Journal of the European Ceramic Society*, 1990, **6**, 3–8.
- 69 X. Li, J. Wang, H. Ji and X. Xu, *Aerospace Materials and Technology*, 2016, **42**, 95–98.
- 70 X. Wan, G. Zhang, O. Ostrovski and H. Aral, *Faculty of Engineering and Information Sciences - Papers: Part A*, 2013, 739–748.
- 71 F. Yan, Y. D. Zheng, P. Chen, L. Sun and S. L. Gu, *Optical Materials*, 2003, **23**, 113–116.
- 72 A. Parrillo, G. Sánchez and A. B. Alles, *SN Appl. Sci.*, 2021, **3**, 268.
- 73 K. R. Carduner, S. S. Shinozaki, M. J. Rokosz, C. R. Peters and T. J. Whalen, *Journal of the American Ceramic Society*, 1990, **73**, 2281–2286.
- 74 K. J. D. MacKenzie and M. E. Smith, Eds., in *Pergamon Materials Series*, Pergamon, 2002, vol. 6, pp. 201–268.
- 75 K. J. D. MacKenzie, *Solid State Ionics*, 2004, **172**, 383–388.
- 76 P. J. Baxter, C. Bonadonna, R. Dupree, V. L. Hards, S. C. Kohn, M. D. Murphy, A. Nichols, R. A. Nicholson, G. Norton, A. Searl, R. S. J. Sparks and B. P. Vickers, *Science*, 1999, **283**, 1142–1145.
- 77 D. G. Nair, A. Fraaij, A. A. K. Klaassen and A. P. M. Kentgens, *Cement and Concrete Research*, 2008, **38**, 861–869.
- 78 R. Ghita, C. Logofatu, C.-C. Negrila, F. Ungureanu, C. Cotirlan, A.-S. Manea, M.-F. Lazarescu and C. Ghica, in *Crystalline Silicon - Properties and Uses*, ed. S. Basu, IntechOpen, 2011.

- 79 T. N. Taylor, *Journal of Materials Research*, 1989, **4**, 189–203.
- 80 K.-H. Lee, S.-K. Lee and K.-S. Jeon, *Applied Surface Science*, 2009, **255**, 4414–4420.
- 81 M. Grodzicki, R. Wasielewski, S. A. Surma and A. Ciszewski, *Acta Physica Polonica A*, 2009, **116**, 4.
- 82 H. A. Bland, E. L. H. Thomas, G. M. Klemencic, S. Mandal, D. J. Morgan, A. Papageorgiou, T. G. Jones and O. A. Williams, *Scientific Reports*, 2019, **9**, 2911.
- 83 Z. Zhu, F. Liang, Z. Zhou, X. Zeng, D. Wang, P. Dong, J. Zhao, S. Sun, Y. Zhang and X. Li, *J. Mater. Chem. A*, 2018, **6**, 1513–1522.
- 84 Y. Zhu, M. Chen, Q. Li, C. Yuan and C. Wang, *Carbon*, 2017, **123**, 727–734.
- 85 E. Bódis, I. Cora, P. Németh, O. Tapasztó, M. Mohai, S. Tóth, Z. Károly and J. Szépvölgyi, *Ceramics International*, 2019, **45**, 4810–4816.
- 86 G.-R. Yang, Y.-P. Zhao, Y. Z. Hu, T. Paul Chow and R. J. Gutmann, *Thin Solid Films*, 1998, **333**, 219–223.
- 87 S. M. Castanho and R. Moreno, *Cerâmica*, 1998, **44**, 141–145.
- 88 X. Sun, H. T. Liu and H. F. Cheng, *RSC Adv.*, 2017, **7**, 47833–47839.
- 89 X. Hu, C. Shao, J. Wang and H. Wang, *J Mater Sci*, 2017, **52**, 7555–7566.
- 90 C. Zou, C. Zhang, B. Li, S. Wang, Z. Xie and Y. Song, *Materials Science and Engineering: A*, 2015, **620**, 420–427.
- 91 *Journal of Cleaner Production*, 2017, **157**, 213–221.
- 92 J. V. Milewski, F. D. Gac, J. J. Petrovic and S. R. Skaggs, *J Mater Sci*, 1985, **20**, 1160–1166.
- 93 A. Chrysanthou, P. Grieveson and A. Jha, *J Mater Sci*, 1991, **26**, 3463–3476.
- 94 Y. Li, Q. Wang, H. Fan, S. Sang, Y. Li and L. Zhao, *Ceramics International*, 2014, **40**, 1481–1488.
- 95 X. K. Li, L. Liu, Y. X. Zhang, Sh. D. Shen, S. Ge and L. C. Ling, *Carbon*, 2001, **39**, 159–165.
- 96 F. Béguin, F. Chevallier, C. Vix-Guterl, S. Saadallah, V. Bertagna, J. N. Rouzaud and E. Frackowiak, *Carbon*, 2005, **43**, 2160–2167.
- 97 H. Zheng, Q. Qu, L. Zhang, G. Liu and V. S. Battaglia, *RSC Advances*, 2012, **2**, 4904–4912.

- 98 H. Fujimoto, K. Tokumitsu, A. Mabuchi, N. Chinnasamy and T. Kasuh, *Journal of Power Sources*, 2010, **195**, 7452–7456.
- 99 G. Li, T. Ouyang, T. Xiong, Z. Jiang, D. Adekoya, Y. Wu, Y. Huang and M.-S. (Jie T. Balogun, *Carbon*, 2021, **174**, 1–9.
- 100K. Ye, K. Li, Y. Lu, Z. Guo, N. Ni, H. Liu, Y. Huang, H. Ji and P. Wang, *TrAC Trends in Analytical Chemistry*, 2019, **116**, 102–108.